JOURNAL OF GEOPHYSICAL RESEARCH, VOL. 96, NO. B12, PAGES 19,733–19,748, NOVEMBER 10, 1991

Fluid Inclusions and Hydrothermal Alteration on the Dixie Valley Fault, Nevada

W.T. PARRY, D. HEDDERLY-SMITH, AND R. L. BRUHN

Department of Geology and Geophysics, University of Utah, Salt Lake City

Footwall rocks of the 1954 rupture segment of the Dixie Valley fault show extensive hydrothermal alteration related to fluids that were present on the fault during tectonic events. Hydrothermal alteration of granitic host rocks consists of temporally and spatially overlapping mineral assemblages. An early, biotite-feldspar assemblage is followed by later Fe-chlorite and epidote. Both chlorite and epidote are replaced by hydrothermal sericite and cross-cut by calcite-hematite and quartz-calcite veins. Biotite is partially replaced by prehnite. The latest hydrothermal minerals are stilbite, laumontite, kaolinite, alunite, smectite, illite, and pervasive replacement of rock units with fine grained quartz, chalcedony, and opal. Secondary fluid inclusions trapped in healed microfractures in igneous quartz include type I inclusions that contain a moderate salinity aqueous liquid and vapor, type II inclusions that contain a moderate salinity aqueous liquid and CO_2, type III inclusions that show eutectic melting temperatures below the NaCl-H_2O eutectic and contain substantial $CaCl_2$, and type IV inclusions containing halite and other daughter minerals. Microthermometric measurements on these inclusions yield variable compositions and homogenization temperatures. Salinities of type I inclusions vary from 0.1 to 12.9 wt % NaCl with the mode in the interval 0 to 1%. Salinities of type II CO_2 bearing inclusions range from 0.62 to 6.81 wt % NaCl relative to H_2O, and salinities of type III inclusions with low eutectic melting temperatures are 12.9 to 25.3 NaCl equivalent wt %. Salinities of halite-bearing inclusions are 30.1 to 39.2 wt % NaCl. Homogenization temperatures span the range 120° to 400°C. The processes of isochemical cooling with upward displacement of the footwall, mixing of cool low-salinity water with hotter components, and mixing of cool, evaporite brine with hotter components could be responsible for variable fluid inclusion compositions, homogenization temperatures, and densities. The P-T path of the fault fluids is established by mineral equilibria and fluid inclusion characteristics. The path includes a lithostatic fluid pressure at 305°C and 1570 bars. Along with cooling and escape of CO_2 from fluids, the fluid P-T path probably approaches hydrostatic pressure conditions at lower temperatures. Hydrothermal alteration product minerals, fluid temperatures, pressures, and compositions in the footwall of the Dixie Valley fault constrain minimum fault age to 20 to 25 Ma, displacement to 6 km with about 3 km of pre-10 to 13 Ma and 3 km of post-10 Ma uplift. Fluid compositions and P-T data suggest the following mechanism for rupture initiation and arrest. Ruptures may be initiated as a result of high fluid pressures, then opening of dilatant fractures causes drastic decrease in fluid pressure, separation of steam and CO_2. The drastic reduction in fluid bulk modulus that accompanies volatile phase separation permits propagation of the ruptures even though fluid pressure is reduced. In areas where fluid pressure reduction is not accompanied by phase separation, fractures are arrested by dilatant hardening.

INTRODUCTION

Hydrothermal fluids play a significant role in the mechanical stability of faults. Increased fluid pressure reduces the frictional shear strength of an existing fault where failure is governed by effective stress [*Hubbert and Rubey*, 1959]. Alteration of the fault rock to mineral assemblages such as muscovite with lower frictional or flow strength decreases stability [*Janecke and Evans*, 1988; *Kirby and Kronenberg*, 1987]. Increased pore volume produced during dynamic rupturing with accompanying reduction in fluid pressure [*Ismail and Murrell*, 1976; *Rudnicki and Chen*, 1988; *Roeloffs and Rudnicki*, 1985], and healing and sealing of cracks with precipitated minerals increase stability. Fault stability is also related to the temperature and pressure of the fault zone and the constitutive properties of fault zone rock and fluids. New pore volume produced by dilatancy coupled with low rock permeability can result in decompression of the fluid and may stabilize rupture. Separation of the fluid into gas and liquid phases results in drastic reduction in fluid bulk modulus that diminishes the dilatant hardening effect and may permit rupture propagation [*Rudnicki and Chen*, 1988; *Parry and Bruhn*, 1990].

Paper number 91JB01965.
0148-0227/91/91JB-01965$05.00

Evidence of hydrothermal fluid circulation and chemical interaction of fluids with fault zone rocks is evident in fault zones exhumed by erosion [*Sibson*, 1981; *Sibson et al.*, 1988; *Parry et al.*, 1988] Microscopic to megascopic fractures filled with precipitated minerals are common, and fluid inclusions trapped within these minerals represent samples of the pore fluids. Characteristics of fluid inclusions together with associated hydrothermal alteration product minerals may be used to infer the physical state of the fault zone at depth, estimate constitutive properties of fault zone materials such as fluid bulk modulus which control fault stability [*Parry and Bruhn*,1990], constrain the fluid pressure [*Parry and Bruhn*, 1986; *Parry et al.*, 1988; *Parry and Bruhn*, 1990], and estimate fault displacement using pressure and temperature constraints [*Parry and Bruhn*, 1987].

The Dixie Valley fault system is part of a 300-km-long active seismic belt in central Nevada [*Wallace*, 1984] with individual segments capable of producing magnitude 7 earthquakes. Exhumed footwall rocks on segments of this fault display the effects of hydrothermal alteration and provide an opportunity for observation of fluid characteristics in fluid inclusions and alteration product mineralogy near seismogenic depths on the fault.

The objectives of this study are to characterize and map hydrothermal alteration assemblages on the footwall of the 1954 rupture segment of the Dixie Valley fault Nevada, to determine the characteristics of fault pore fluids using fluid inclusions and

alteration mineralogy, and to relate these characteristics to fault behavior and history. We have chosen the 1954 rupture segment for study because the footwall exposes Tertiary age granitic rocks in which alumino-silicate minerals provide an excellent record of chemical interaction of fluids and because the age of the alteration must postdate the emplacement of the igneous host rock.

THE DIXIE VALLEY FAULT

The Dixie Valley fault in the western Basin and Range province of Nevada lies in an area of high heat flow, late Cenozoic volcanic activity, and recent seismic activity. Historic seismicity has resulted in surface rupturing events (from north to south) at Pleasant Valley (1915), Fairview Peak-Dixie Valley (1954), Wonder (1903), Cedar Mountains (1932), Excelsior Mountain (1934), Mammoth Lakes (1980), and Owens Valley (1972) [*Wallace and Whitney*, 1984].

The Dixie Valley fault system forms the eastern margin of the Stillwater Mountains shown in Figure 1, and close spatial correlation between the 1954 and older fault scarps indicates that repeated surface-rupturing earthquakes have created the structural relief between the Stillwater mountains and Dixie Valley. Footwall rocks exposed in the Stillwater range shown in Figure 1 include Mesozoic sedimentary rocks intruded by the Jurassic gabbroic Humboldt lopolith [*Willden and Speed*, 1974] a multiphase Oligocene granodiorite-quartz monzonite-granite intrusion emplaced at 28 Ma [*Speed and Armstrong*, 1971], and a small Cretaceous granitic intrusion. These rocks are overlain by Tertiary volcanic rocks.

Dixie Valley is a graben system consisting of an inner graben with valley fill 2 to 3.2 km deep and a shallower outer graben containing 150 to 1500 m of fill [*Meister*, 1967; *Thompson and Burke*, 1973; *Okaya and Thompson*,1985; *Anderson et al.*, 1983]. Fault displacement has taken place along a normal fault at the base of the Stillwater range (the range front fault) and along a zone of normal faults a few km east of the range front (the piedmont fault zone) [*Bell and Katzer*, 1987, 1990]. Small scarps of the Piedmont fault zone shown on Figure 1 mark the innter graben.

The topographic low in Dixie Valley is dominated by a large playa and the Humboldt salt marsh occupies 46 square miles (119 km^2) of Dixie Valley at an elevation of 3365 feet (1026m) [*Bateman and Hess*, 1978]. The brine is 28.7 to 38.7 wt % salt.

EXPERIMENTAL PROCEDURES

Our studies focus on hydrothermal alteration and fluid inclusion characteristics in footwall granitic and volcanic rocks of the 1954 rupture segment of the Dixie Valley range front fault. Samples were collected from outcrop of the intrusive and volcanic rocks in the footwall of the Dixie Valley fault at localities shown in Figures 2a, 2b, and 2c. Hydrothermal alteration mineral assemblages, tectonic textures, and fluid inclusions were studied in 183 thin sections of rocks collected during the course of mapping footwall alteration. Alteration mineralogy and tectonic textures were determined by a combination of petrographic microscope and X ray diffraction techniques. Clay minerals were identified by X ray diffraction of oriented smears of clay size material following vapor glycolation at

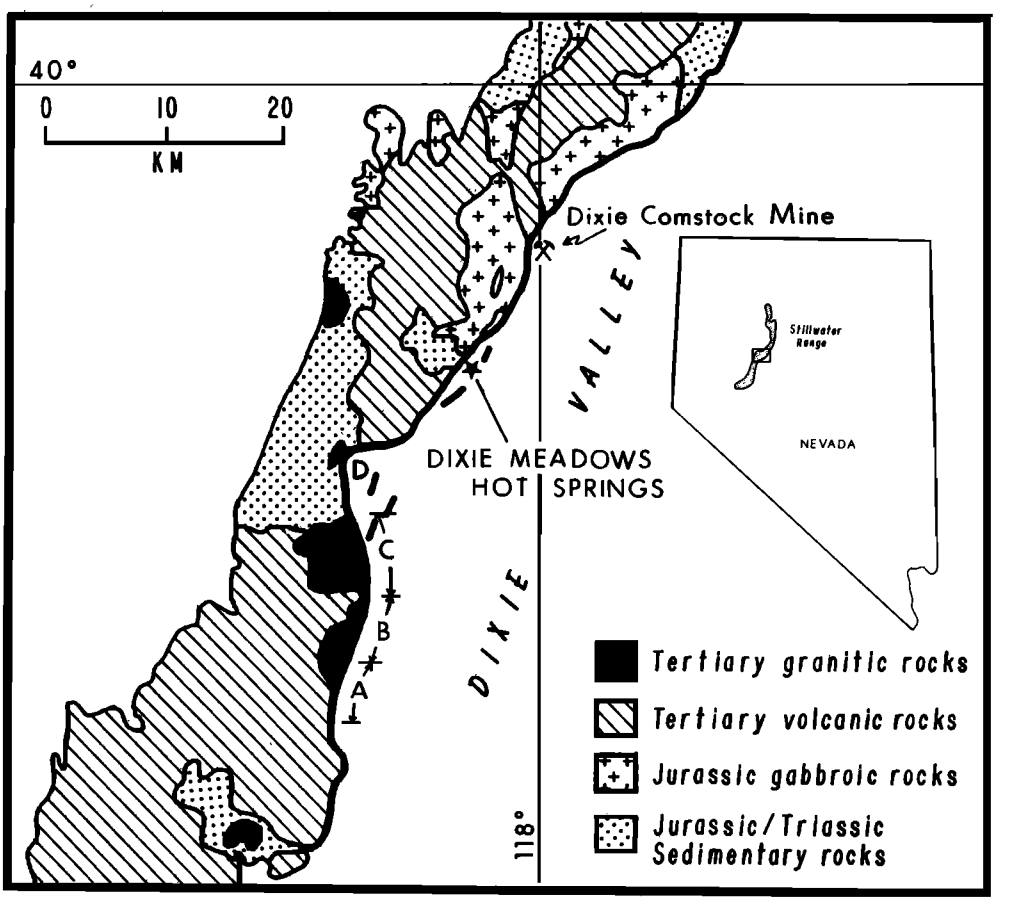

Fig. 1. Index map of Nevada showing the Stillwater Mountain Range and generalized geologic map of a portion of the Stillwater Mountain range modified from *Page* [1965] The range front fault is shown as a heavy line. A, B, and C are sections of the Dixie Valley fault and footwall shown in detail in Figure 2.

60°C and heating to 250° and 550°C. The relative ages of alteration assemblages is established from crosscutting and replacement relationships.

Identity, density, and homogenization temperatures of fluid inclusion contents were determined by observation of phase changes in doubly polished plates on a Fluid Incorporated heating-freezing microscope stage and procedures outlined by *Roedder* [1984], *Parry and Bruhn* [1986], *Parry* [1986] and *Parry et al.* [1988]. Temperature calibration for the microscope stage was accomplished using synthetic fluid inclusions of known composition [*Sterner and Bodnar*, 1984]. Phase changes that were used to characterize fluid inclusion fluids were the CO_2 triple point temperature; melting of clathrate [*Collins*, 1979; *Bozzo et al.*, 1975]; melting of ice, hydrohalite, and halite; CO_2 liquid-vapor homogenization; and overall homogenization of fluid inclusion contents.

Fluid inclusion salinities were estimated from ice melting temperatures, from clathrate melting temperatures, and from halite melting temperatures as appropriate. Salinities of fluids in inclusions with no detectable CO_2 were calculated using freezing point depression estimated from ice melting temperatures and the regression equation of *Potter et al.* [1978]. Salinities for fluid inclusions on the halite liquidus were calculated using the equation and coefficients of *Sterner et al.* [1988]. Salinity of fluid inclusions showing eutectic temperatures below the NaCl-H_2O eutectic were estimated using the equations and coefficients for total salinity of *Oakes et al.* [1990].

The greatest source of error in fluid inclusion measurements is a consequence of post entrapment changes in secondary inclusions described as necked inclusions by *Roedder* [1984] and termed maturation by *Bodnar et al.* [1985]. These changes result from dissolution and reprecipitation of host mineral surrounding the trapped fluid. The initial fluid inclusion may be irregularly shaped but in time necks down to form many smaller inclusions with more regular shapes. If necking takes place after separation of a vapor phase, then the result is varying liquid to vapor ratios. All secondary fluid inclusions have undergone necking, but generally, the necking takes place before separation of a vapor phase or other daughter phases [*Roedder*, 1984]. We have avoided measurements of fluid inclusions with liquid-vapor ratios affected by necking using the following procedures: first, fluid inclusions in close proximity to one another with widely varying liquid to vapor ratios were not measured; second, inclusions near one another with apparently similar liquid-vapor ratios were checked to insure similar homogenization temperatures.

FAULT ROCK PETROGRAPHY AND ALTERATION

Four separate plutons in the intrusive complex shown in Figures 1 and 2 were recognized in the footwall of the 1954 rupture segment during our field investigations, but the contacts between these plutons were not mapped. They are, from south to north, granite (40% plagioclase, 33% K-feldspar, 25%quartz, 2% biotite) outcropping in the vicinity of A in Figure 1; granodiorite (62% plagioclase, 12% K-feldspar, 19% quartz, 7% biotite) outcropping in the vicinity of B in Figure 1; biotite quartz monzonite (26% plagioclase, 34% K-feldspar, 27% biotite, 8% hornblende, 9% quartz) outcropping in the vicinity of C in Figure 1; and a small granite to granodiorite stock near Alameda Canyon (D on Figure 1) that consists of 33% quartz, 43% plagioclase, 17% K-feldspar, and 7% biotite. The K-Ar age of biotite from the biotite quartz monzonite at locality 108, Figure 2c, is 28±2 Ma (Table 1) [*Speed and Armstrong*, 1971]. The granite is younger than the granodiorite, but the relative age of the granodiorite with respect to the biotite quartz monzonite is not known due to the lack of outcrop. The K-Ar age of muscovite from the Alameda Canyon pluton at D on Figure 1 is 78.4±2.9 Ma (Table 1). Additional smaller intrusive rocks are also present at map localities shown in Figure 2 and include an altered quartz latite porphyry dike at 37, a diorite dike at 17, a quartz diorite dike at 65 and a diorite dike at 97. These smaller bodies are too small to map at the scale of Figure 2.

Fault breccia and cataclasite developed within the granitic protolith directly overlie the footwall granitic rocks. A pervasive set of closely spaced extension fractures is concentrated in the footwall immediately adjacent to the fault. Spacing between these steeply east dipping extension fractures is only a few centimeters and these fractures are present throughout the breccia and within the footwall for several meters to tens of meters. Thin discontinuous shear planes subparallel to the main fault plane also extend into the footwall and coexist with the penetrative fracture set.

Cataclasite is the dominant fault rock. Cataclastic textures include pervasive fracturing of large volumes of rock and veins. Cataclastic veins are thin tabular and branching bodies of fine cataclasite

TABLE 1. Potassium-Argon Age Data

Map No	Sample	Description	Dated Mineral	K, wt %	$^{40}Ar^*/^{40}Ar$ Total, %	$^{40}Ar^*$, x10-10mol/g	Age, Ma±σ
108	IXL Pluton	fine to coarse plag K-feldspar, quartz 30°41'27"N 118°08'02"W	biotite	6.91	69	3.40	28±2.0
D	DV87-59	very coarse muscovite +quartz vein in granite	muscovite	8.91	82.1 89.7	12.37	78.4±2.9
18	DV87-7	sericite completely replacingfeldspars in granite	muscovite	7.72	26.5 35.3	3.37	25.0±1
20	DV87-5b	near quantitative replacement of feldspares in granite	muscovite	7.07	54.6	2.69	21.8±0.9

Analyses by Geochron Laboratories. $\lambda\beta=4.962\times10^{-10}$/yr. $\lambda\varepsilon+\lambda\varepsilon'=0.581\times10^{-10}$/yr. $^{40}K/K=1.193\times10^{-4}$g/g. $^{40}Ar^*$=radiogenic Ar.

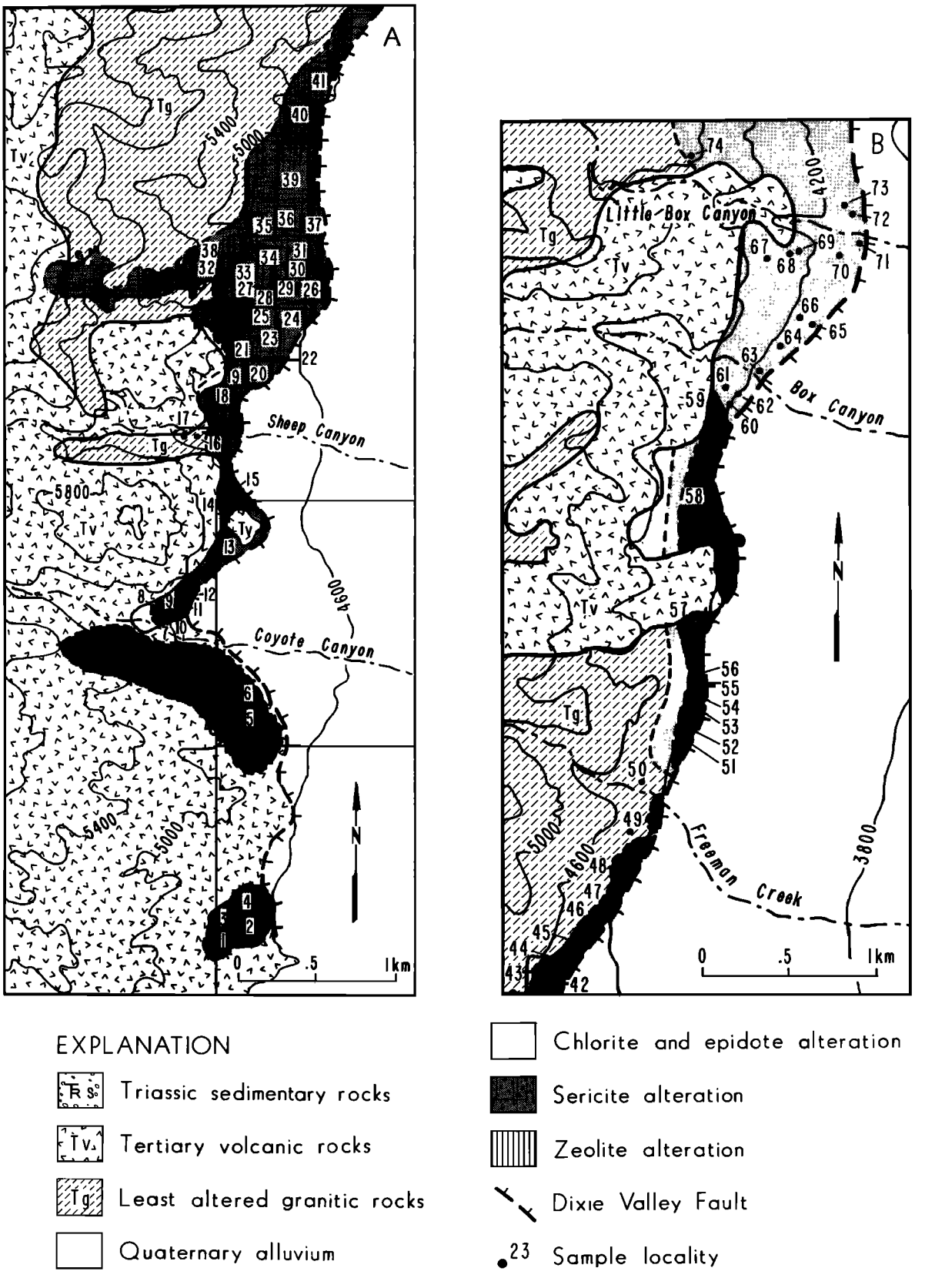

Fig. 2. Geologic, alteration, and sample location map of portions of the Dixie Valley fault. Temporally and spatially overlaping hydrothermal alteration mineral assemblages in footwall rocks are shown. (a) Coyote Canyon area, (b) Box Canyon area, and (c) IXL Canyon area.

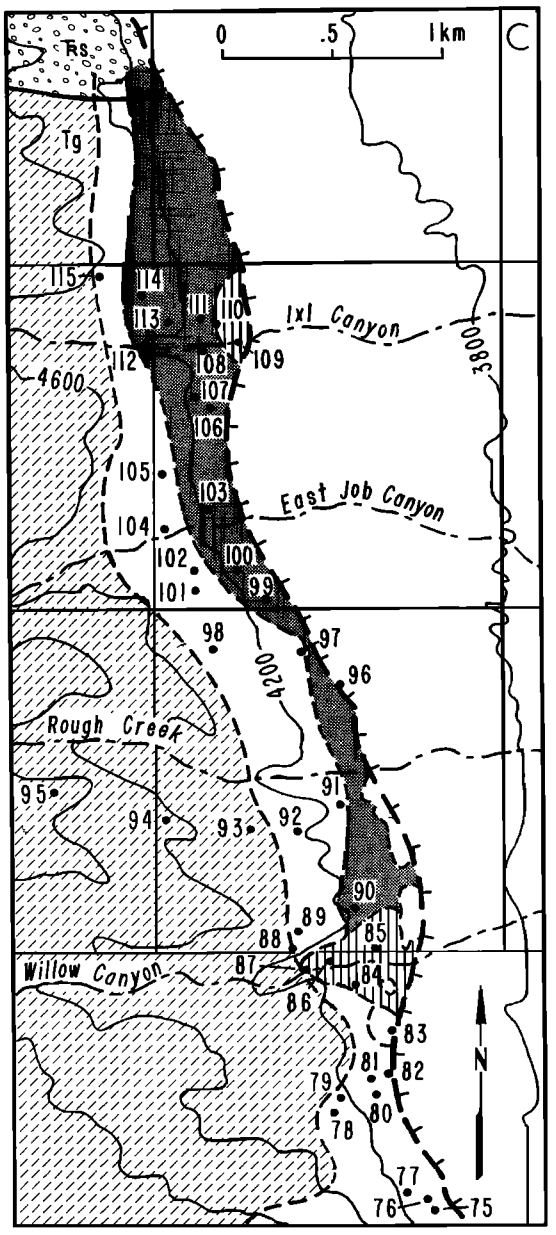

Fig. 2. (continued)

consisting of angular fragments of quartz and feldspar occasionally with a matrix of sericite or chlorite. No shear displacement of the fracture walls is apparent in thin section even though the fractures are crowded with angular fragments of quartz and feldspar and the quartz may be stretched and recrystallized. We infer that the cataclasite was emplaced as a suspension of fine rock particles possibly during hydraulic fracturing.

Temporally and spatially overlapping hydrothermal alteration mineral assemblages occur as a narrow band near the 1954 rupture in the fault footwall. Geometric association of the alteration with the fault and association with tectonic textures indicate alteration mineral assemblages are related to tectonic events on the Dixie Valley fault. From earliest to latest, these assemblages are biotite+K-feldspar, chlorite+epidote, sericite+kaolinite+ smectite, prehnite+laumontite+ stilbite+kaolinite+smectite. The spatial distribution of areas dominated by sericite, chlorite+epidote, and zeolite assemblages is shown in Figure 2. The sericitic alteration is superimposed on chlorite and epidote, traces of which remain in the rock. Prehnite, laumontite, stilbite, and clay minerals have also been superimposed on earlier alteration mineralogies with traces of the earlier minerals remaining in the rock.

The earliest assemblage of hydrothermal minerals includes a pervasive, partial to complete replacement of igneous plagioclase by K-feldspar, leaving patchy remnants of twinned plagioclase crosscut by K-feldspar veins visible in thin sections. Hydrothermal K-feldspar also occurs as selvages on quartz veins and as quartz+K-feldspar veins. Later veins of albite also crosscut plagioclase. Hydrothermal K-feldspar was not mapped but is widely distributed along the fault footwall. Hydrothermal biotite also forms early in the sequence, though the relative age of biotite cannot be unequivocally tied to the K-feldspar replacement of plagioclase. Hydrothermal biotite occurs as thin veins, as replacement of hornblende and as a replacement of igneous biotite. Hydrothermal biotite is more abundant in more mafic rocks where biotite vein networks occur in plagioclase and pyroxene. Hydrothermal biotite is not volumetrically abundant any where in the fault footwall.

The dominant alteration mineralogy on the Dixie Valley fault footwall is Fe-chlorite and epidote associated with local areas of calcite, hematite, sericite, and prehnite. Chlorite replaces hornblende and biotite and occurs in veins with actinolite, green biotite, calcite, quartz, or epidote. Epidote forms a selvage to quartz+epidote veins that reach thicknesses of several centimeters. Cataclasite and breccia consisting of epidote and chlorite form the faces of some of the faceted spurs.

Hydrothermal sericite (dioctahedral white mica) replaces all previously formed minerals except quartz. In the most intense sericitic alteration, feldspars have been nearly completely replaced by sericite and fine-grained quartz . The resulting altered rock consists of up to 58% sericite, relict igneous quartz, and fine-grained hydrothermal quartz. Biotite, hornblende, chlorite, and epidote are completely replaced by sericite. With decreasing intensity of alteration sericite occurs as disseminated grains within the feldspars and as isolated veins. X ray diffraction of clay-sized separates from sericitized rocks shows both kaolinite and smectite associated with the sericite. However, thin section examination shows the kaolinite and smectite are later than the sericite.

Prehnite occurs locally as fibrous, radiating masses with typical bow-tie extinction which partially replaces biotite.

Latest hydrothermal minerals are laumontite, stilbite, kaolinite, smectite, and very fine grained illite that occur on the fronts of faceted spurs at exposures of the 1954 rupture trace of the range front fault (Figure 2c). Silicification of both volcanic and plutonic rocks is the latest alteration event. Chalcedony, kaolinite, alunite, smectite, and opal occur in volcanics both north and south of the 1954 rupture segment.

Deep exploration wells in northern Dixie Valley crossed the Dixie Valley fault. Well data indicate that volcanic and alluvial material is altered to albite, chlorite, illite, epidote, and clay. Plagioclase is altered to albite, illite, epidote, calcite, and clay, and hornblende is altered to biotite, chlorite, magnetite, epidote, and calcite. In the meta sediments, illite forms from andalusite, and biotite alters to vermiculite and calcite. Quartz, laumontite, and adularia veins are observed [*Bell et al.*, 1980].

JOINT AND VEIN SYSTEMS

Mineral assemblages precipitated in veins and on joint surfaces occur in several sets of variably oriented fractures that formed over an extended period of time. The youngest mineral assemblages consist of prehnite-laumontite-stilbite-clay, and calcite-filled

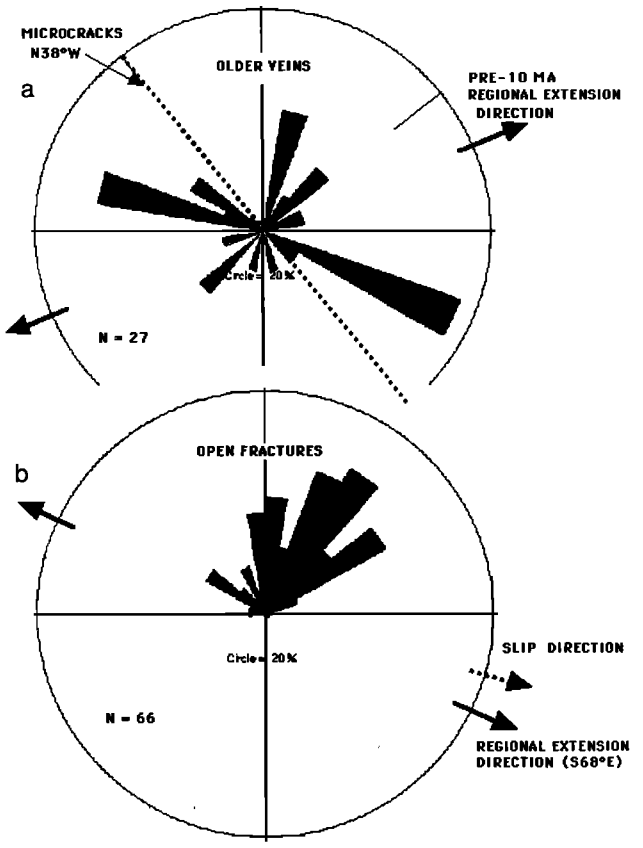

Fig. 3. (a) Rose diagram of strike directions of open fractures on the Dixie Valley fault, Nevada. (b) Rose diagram of strike directions of hydrothermal veins.

veinlets. This assemblage is concentrated in north to NE trending fractures that parallel the Dixie Valley fault trace (Figure 3a). Sericite-clay and older mineral assemblages are concentrated in NW to WNW striking veins that strike at a high angle to the contemporary fault zone and in a secondary set of NNE to NE striking veins (Figure 3b). These older mineral assemblages form bands of alteration several tens to hundreds of meters wide that either parallel the Dixie Valley fault zone or cut into the footwall at a high angle to the fault zone (Figures 1 and 2). Two samples of hydrothermal sericite were dated using the K-Ar method; one yielded an age of 21.8 Ma and the other 25 Ma (Table 1), indicating that this alteration occurred during late Oligocene to early Miocene.

The sericite-clay alteration assemblage is younger than the chlorite-epidote and biotite-K-feldspar assemblages based on crosscutting relationships seen in the field and in thin section. The epidote-chlorite assemblage is best preserved from Little Box Canyon to Willow Canyon (Figure 2), but remnants of this assemblage extend along almost the entire length of the fault zone in the study area. In most locales along the range front, the sericite-clay assemblage overprints the epidote-chlorite mineralization. Near Sheep Canyon, in the southern part of the study area (Figure 2), sericite-clay mineralization extends about 1 km into the footwall along a closely spaced set of WNW to west striking joints and veins.

Orientations of mineral-filled veins suggest that an early stage of activity on the Dixie Valley fault with an ENE to WSW extension direction is associated with mineral-filled extension veins of quartz, epidote, quartz-sericite, clay minerals, and hematite. Fractures with dustings of euhedral quartz, stilbite, chlorite, calcite, epidote, and hematite are parallel to present-day extension fractures.

FLUID INCLUSION PETROGRAPHY

Healed microcracks in both igneous quartz and vein quartz contain thin planar trails of numerous secondary fluid inclusions that often crosscut boundaries between adjacent quartz grains. In least altered rocks there are a few trains of small (<1μm) fluid inclusions, but most quartz grains near the fault show many intersecting planar arrays of secondary fluid inclusions. While numerous intersections of fluid inclusion trains are apparent, it is not possible to determine a fluid inclusion chronology from crosscutting relationships. Necking is a common phenomena. Fluid inclusions appear as irregular, immature to very regular mature inclusions with negative crystal shapes. Nearby fluid inclusions in linear arrays that are mature and display negative crystal outlines often have similar liquid to vapor ratios sugggesting that necking preceded separation of a vapor phase.

The abundance of secondary fluid inclusions larger than 1μm can be correlated with proximity to the mapped trace of the Dixie Valley fault. Quartz grains nearest the fault trace contain up to $2x10^5$ fluid inclusions per cubic millimeter. Fluid inclusion abundance decreases to $3x10^4$ fluid inclusions per cubic millimeter within 6 m of the fault at Coyote Canyon and 400 m of the fault at IXL canyon. Here the broader distribution is due to the presence of several subsidiary faults.

Arrays of secondary fluid inclusions are subparallel to cataclastic veins with a second set at high angles to cataclastic veins. The orientations of fluid inclusion trails that define partly healed microfractures were measured on oriented samples of granitic rock using a universal stage (Figure 4). Poles to these trails are shown in Figure 4 contoured in terms of standard deviations (σ) from a uniform distribution of points. Three areas of high point density are apparent. The most prominent crack orientation, point density of 8-10σ, represents nearly vertical planes striking N38°W about 15°

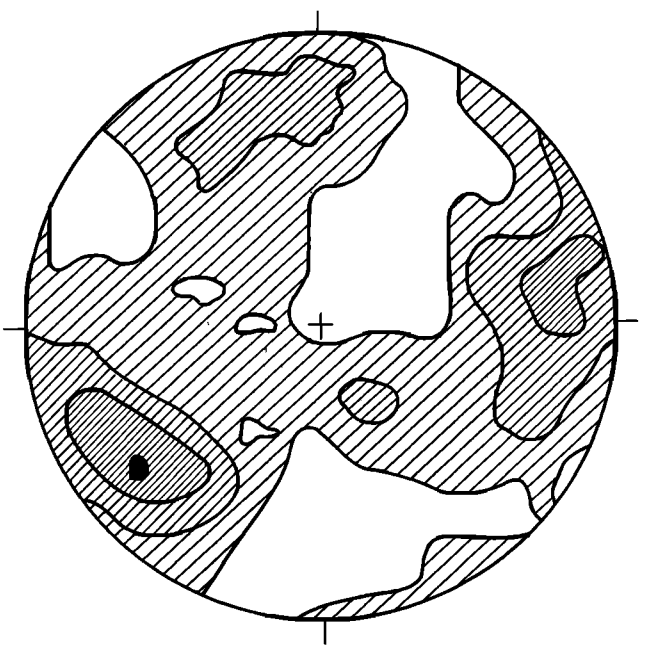

Fig. 4. Equal-area stereographic plot of poles to fluid inclusion trails, lower hemisphere. Contoured in terms of standard deviations from a uniform distribution of points [*Kamb*, 1959] with the contour interval of 2σ indicated by width of ruled lines. A uniform distribution is represented by 3σ, so the unruled area representing 2σ-4σ represents the area of the diagram in which the counting circle contained a distribution of points equivalent to 1σ on either side of the density of a uniform distribution of points.

TABLE 2. Characteristics of Major Fluid Inclusion Groups

Property	Type I Moderate Salinity	Type II CO_2-Bearing	Type III Low Eutectic	Type IV Halite
Phases at room temperature	40-90%l 10-60%v	60-90% H_2Ol 10-40% CO_2l +CO_2v	80-90%l 6-20%v	H_2Ol H_2Ov 2-10% NaCl
Aqueous phase at low temperature	freeze at -30° to-40°C melting of last solid (ice) 0° to -11°C		freeze at -60° -80°C coarsens -40°C visible melt -40°C melting of last solid ice -26° to -9°C	
Bubble behavior at low temperature	no change	CO_2 melts -57.5° to -54.4°C		
Gas hydrates	none	clathrate melts 6.4° to 9.7°C		
Heating behavior	homogenization to l at 125°-400°C	CO_2 l-v 22.5°-29.3°C(v) CO_2 l-v 25.4°-29.4°C(l) homogenization to l at 197°-358°C	homogenization to liquid 129°-283°C	TmNaCl 160°-356°C Thl-v 275°-382°C
Number of measurements	256	45	17	7

v, homogenizes to vapor phase; l, homogenizes to liquid phase.

clockwise of the dominant NW to WNW concentration of older veins observed in outcrop. The next most prominent, 6-8σ, represents planes N10°W and the third set, 4-6 σ, represents planes striking N72°E.

The K-Ar age of hydrothermal illite in the area is 21 to 25 Ma (Table 1) corresponding to the earlier episode of extension where the extension direction is WSW-ENE consistent with mode I microcracks hosting fluid inclusions striking N38°W. Fluid inclusion fluids on this section of the Dixie Valley fault must therefore be associated with the early phase of Basin and Range extension. The orientations of fluid inclusion trails are subperpendicular to the inferred Oligocene to early Miocene regional stress field.

FLUID INCLUSION MEASUREMENTS

Phase changes observed in fluid inclusions on the heating-freezing microscope stage have revealed a diverse assemblage of chemically distinct fluids on the Dixie Valley fault. Fluid inclusions are categorized by their contents into liquid+vapor, moderate salinity inclusions (type I); carbon dioxide bearing inclusions (type II); low eutectic temperature inclusions (type III); halite bearing inclusions (type IV); and one-phase (liquid) inclusions. A few inclusions contain solid phases in addition to halite. The one-phase (liquid) inclusions are the youngest. The thermometric measurements are summarized in Table 2. The majority of fluid inclusions measured consist of an aqueous phase and a vapor bubble usually comprising 10 to 30 vol % (type I). Ice is the last phase to melt on warming. A second and possibly related type of inclusion contains a large vapor bubble (more than 60 vol %) and a small volume of low-salinity liquid. These two types of inclusions are occasionally in close proximity to one another and may show similar homogenization temperatures, the first to liquid and the second to vapor. These characteristics could be considered evidence for boiling of fluids at some stage of fault development. However, the widespread occurrence of necked inclusions suggests that necking probably accounts for this association. CO_2-bearing inclusions (type II) are present on some sections of the fault.

Two types of high-salinity inclusions are present. A few inclusions consisting of only vapor and liquid showed eutectic temperatures well below the NaCl-H_2O eutectic (type III). The fourth type of fluid inclusions contain daughter minerals (type IV). These daughter minerals include an isometric salt probably halite, a small, high-relief unidentified salt, and a platy, birefringent mineral that may be sericite.

Moderate Salinity Inclusions (Type I)

Microthermometric measurements of type I fluid inclusions have revealed wide diversity in chemical composition and homogenization temperatures. Salinities in NaCl equivalent wt % calculated from ice melting temperatures are shown for 265 fluid inclusions in the histogram of Figure 5. Salinity data form a highly skewed distribution with most frequent values in the low salinity range 0 to 1% NaCl. However significant numbers of higher salinity fluid inclusions were observed.

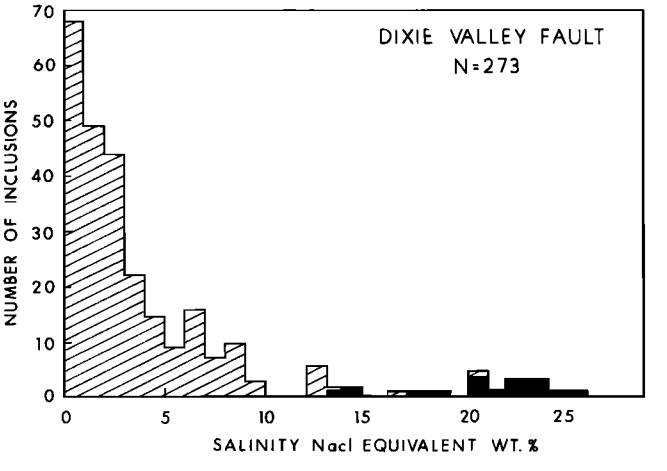

Fig. 5. Histogram of salinities of Type I (ruled lines) and Type III (solid) fluid inclusions calculated from ice melting temperatures using the regression equation of *Potter et al.* [1978].

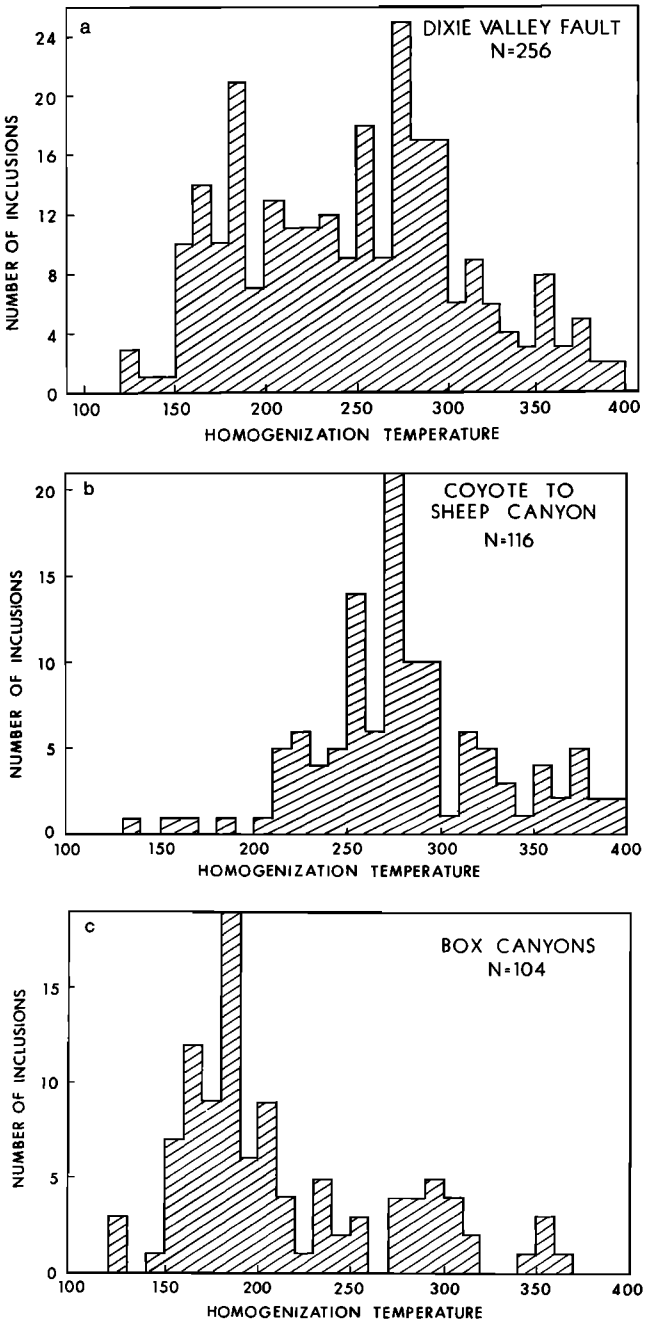

Fig. 6. (a) Homogenization temperatures of type I aqueous fluid inclusions from the Dixie Valley fault footwall. (b) Homogenization temperatures of fluid inclusions from the Coyote Canyon area of Figure 2a. (c) Homogenization temperatures of fluid inclusions from the Box Canyons area (Figures 2b and 2c).

Homogenization of type I fluid inclusions occurred by disappearance of the vapor bubble. The range in homogenization temperatures is 120° to 400°C (Figure 6). The mode of Th values is 270°- 280°C in the southern area near Coyote and Sheep Canyon (Figure 2a) and 180°-190°C in the Box Canyons area (Figure 2b), an area dominated by chlorite and epidote alteration (Figure 6), although both areas have homogenization temperatures that span nearly the full range.

Homogenization temperature is plotted versus salinity for type I, type II, and type III fluid inclusions in Figure 7. The data points on Figure 7 indicate no apparent trends of cooling and dilution. Homogenization temperature and salinity define the fluid density

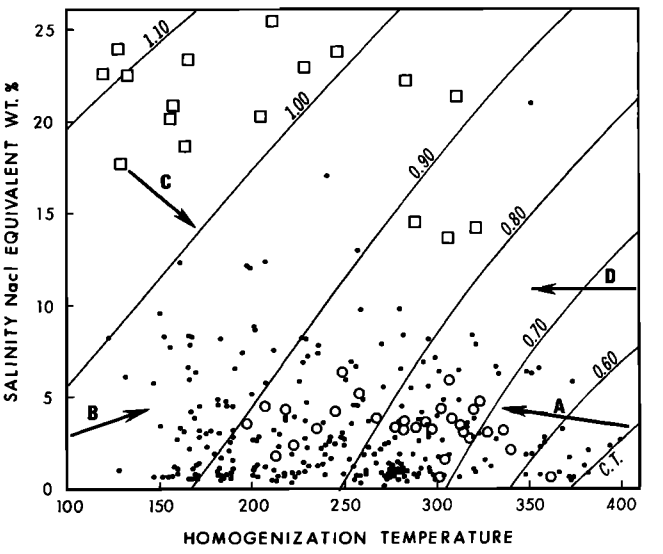

Fig. 7. Temperature of homogenization of fluid inclusions plotted versus salinity. Symbols are open squares, low eutectic inclusions (type III); open circles, CO_2 inclusions (type II); solid circles, moderate salinity aqueous inclusions (type I). Moderate salinity aqueous inclusions (type I) are contoured in terms of density (g/cm3) using the equations and coefficients of *Potter and Brown* [1977]. Density contours do not apply to CO_2 inclusions shown as open circles. Trends in the diagram indicated by arrows and discussed in the text are A, boiling; B, cool, low-salinity water mixing; C, cool evaporite mixing; and D, isochemical cooling of the fault footwall.

and Figure 7 is contoured in terms of density. Because fluids trapped in inclusions are constant density systems, the fluids must be trapped along isochores defined by these density values.

CO2-Bearing Fluid Inclusions (Type II)

Secondary fluid inclusions containing CO_2 are present in several areas of the Dixie Valley fault footwall. These inclusions contain a recognizable meniscus separating liquid CO_2, vapor CO_2, and an aqueous liquid at room temperature. Thermometric properties of these inclusions are shown in Table 3. The liquid CO_2 phase that is frozen by supercooling to below -90°C, melts in the presence of CO_2 vapor at temperatures of -57.6°C to -54.4°C. The most frequent melting temperature is within 0.2°C of -56.6°C, the triple point temperature of pure CO_2. Lower melting temperatures could be accounted for by small amounts of methane. The melting temperatures above -56.6°C can not be accounted for by any known phase equilibria, but these temperatures are reproducible and not the result of experimental error.

Clathrate melting temperatures of CO_2-bearing inclusions yield salinities of 0.62 to 6.8 wt % NaCl relative to H_2O (Table 3). These salinities together with the homogenization temperatures are plotted on Figure 7 for comparison with aqueous inclusions, but the density contours on Figure 7 apply only to the aqueous inclusions.

The CO_2 component of these inclusions homogenized to liquid at 25.4°-29.5°C or to vapor at 20.5°-29.3°C. Homogenization to the liquid implies a greater density of CO_2 and entrapment at higher pressure.

Overall homogenization of CO_2 bearing inclusions occurred over nearly as wide a range (197°-371°C) as the moderate salinity inclusions (Table 2 and Figure 7).

Low Eutectic Temperatures (Type III)

Fluid inclusions with ice melting temperatures between -10.1°C and -26.0°C had very low initial melting temperatures as low as -

TABLE 3. Microthermometric Properties of CO_2-Bearing Fluid Inclusions

Map	Sample	No.	$TmCO_2$	Tm CO_2 Clath	$ThCO_2$ L-V	Th	Volume Percent $\%CO_2$	WNaCl	XNaCl	XH_2O	XCO_2	P, bar
12	DV87-1f	1	-56.5	9.2	28.0v	304	30	1.63	0.005	0.931	0.065	390
		4	-56.9	8.4	20.5v	313	29	3.19	0.010	0.942	0.049	320
		8	-56.8	7.9	26.5v	297	27	4.14	0.012	0.933	0.055	360
		14	-57.4	9.7	27.9v	300	30	0.62	0.002	0.934	0.064	340
		15	-56.4	9.6	29.3v	278	25	0.82	0.002	0.939	0.058	340
		16	-57.6	7.9	28.0v	335	39	4.14	0.012	0.902	0.086	450
		17		9.0	27.1v	340	40	2.03	0.006	0.909	0.085	440
22	DV87-4	17	-56.8		29.4	270v						
		18	-56.7	9.7	22.5v	371v	80	0.62	0.001	0.726	0.272	
		19	-57.2	8.0	28.4l	239D	17	3.95	0.012	0.921	0.068	
20	DV87-5a	8	-56.4			307		3.19				
		11	-57.0	8.5	26.6l	312D	42	3.10	0.008	0.810	0.182	
		12	-57.5	8.5	26.2l	254D	25	3.10	0.008	0.890	0.102	
		13		8.2	29.0l	197	9	3.67	0.011	0.947	0.042	540
18	DV87-7	5	-56.3	8.5	27.2v	312v		3.10	0.009	0.066	0.068	
		6	-56.3	8.5	26.4v	280	23	3.10	0.009	0.943	0.048	350
		7	-56.3	8.1	27.5v	308	31	3.86	0.011	0.924	0.065	380
		8	-56.3	8.6	22.5v	318	32	2.91	0.008	0.935	0.056	340
43	DV87-19	1	-56.4	7.1	24.7v	80v?	90	5.59	0.009	0.479	0.512	
		2	-56.9	6.9	24.0v	210D	15	6.03	0.018	0.948	0.033	
		6	-57.0	6.8	27.5v	250D	26	6.12	0.019	0.926	0.055	
		7	-57.1	7.9	28.0	261D	28	4.14	0.012	0.927	0.060	
D	DV87-54a	1	-55.4	8.5	26.5l	240D	21	3.00	0.009	0.906	0.085	
		2	-55.1	9.1	27.2l	252D	25	1.83	0.005	0.895	0.100	
		3	-54.9	8.1	25.4l	280	31	3.76	0.010	0.856	0.134	1480
		4	-54.4	8.0	27.0l	268	27	3.95	0.011	0.881	0.108	1300
		5	-56.7	7.6	28.7v	324	34	4.69	0.014	0.910	0.076	550
		6	-56.5	7.8	28.4v	320	36	4.32	0.013	0.907	0.080	430
		7	-56.8	7.8	27.5v	303	30	4.32	0.013	0.924	0.063	370
D	DV87-55	1	-56.7	8.3	30.0v	234	14	3.38	0.010	0.950	0.039	360
		3	-56.5	7.7	29.4l	208	10	4.51	0.014	0.939	0.047	670
		5		7.9	29.0v	244	21	4.14	0.012	0.908	0.082	880
D	DV87-59	1	-56.0	7.9	27.5v	219	10	4.14	0.013	0.958	0.030	280
		2	-56.0	9.2	29.5v	216	10	1.63	0.005	0.963	0.032	310
		3	-55.6	8.9	28.9v	222	11	2.22	0.007	0.961	0.033	300
		4	-56.6	8.4	29.4l	279	33	3.19	0.009	0.866	0.126	1060
		5	-56.6	8.4	29.5l	287	32	3.19	0.009	0.866	0.125	1200
		7	-56.7	6.4	24.1l	268D	25	6.81	0.020	0.875	0.105	
		9	-55.2	6.7	27.3l	248	18	6.29	0.019	0.908	0.073	1250
		10	-56.8	7.4	27.6l	259	19	5.05	0.015	0.909	0.076	1380
		11	-56.8	6.9	28.3l	305	32	5.94	0.017	0.857	0.126	1570
		12	-55.6	8.2	26.2l	294	39	3.57	0.009	0.824	0.167	1450

v, homogenizes to vapor phase; l, homogenizes to liquid phase; D, decrepitated. Map number on Figures 1 and 2.

45°C and ice crystal nucleation temperatures as low as -60°C to -80°C. These characteristics suggest the presence of a significant $CaCl_2$ component in the fluid. These fluid inclusions have salinities of 13.6-25.3 wt % $CaCl_2$ +NaCl (Figure 5). In two cases, fluid inclusions were sufficiently large and visible to observe hydrohalite and ice melting temperatures. In these two fluid inclusions the weight fraction NaCl relative to CaCl2 was 0.3 and 0.55. Homogenization of liquid and vapor in fluid inclusions with low eutectic temperatures ranged from 120° to 321°C. Homogenization temperatures and salinities of these inclusions are shown as open squares in Figure 7.

Inclusions Containing Halite (Type IV)

Several fluid inclusions that contain a vapor bubble, a halite crystal and liquid at 25°C were observed. These inclusions homogenize by disappearance of the vapor bubble or by dissolution of the halite crystal. The homogenization of liquid and vapor occurred at a temperature below the halite melting temperature in several of these inclusions. Because halite melting occurred in the presence of liquid only, estimated salinity is only approximate because of the unknown slope of isopleths in P-T space [*Sterner et al.*, 1988].

Fluid inclusions with a halite daughter salt are the highest salinity fluid inclusions. Salinities determined from halite melting temperatures of 160°-297°C for inclusions that homogenize by vapor disappearance are 30.1 to 37.9 NaCl equivalent wt %. In some halite-bearing inclusions, however, halite was present at the temperature of vapor bubble disappearance. Some of these inclusions decrepitated before all halite had dissolved. The few halite-bearing inclusions that homogenized by dissolution of halite yielded salinities of 39.2 to 43 NaCl equivalent wt %.

Discussion

Evidence that fluid inclusions and alteration mineral assemblages represent fluids and their interaction with rocks related to faulting includes occurrence of alteration bands in the fault footwall, spatial orientation of fluid inclusions trails consistent with the stress system producing the faulting, and correlation of fluid inclusion abundance

with proximity to the fault. All fluid inclusions measured and all observed alteration minerals are in the footwall of the Dixie Valley fault, and all postdate the intrusion of the granitic rocks at 28 Ma so that the fluid inclusion fluids and alteration have a maximum age near the inception of extension.

The diversity in salinity of fluid inclusions could result from mixing of low-salinity and high-salinity components. These components may include cool, low-salinity meteoric water, saline water formed in evaporite basins, moderate salinity thermal water, and a high-temperature boiling fluid with temperature and salinity variations caused by steam separation. Lower temperatures resulting from boiling would correspond to higher salinities as shown by the temperature-salinity mixing lines labeled A on Figure 7. Mixing of low-temperature, low-salinity meteoric water with boiling fluids at any stage in their evolution toward lower T and higher salinity is labeled B on Figure 7. The present-day Dixie Valley contains evaporites in Humboldt Salt Marsh, and the extensive evaporites of Carson and Humboldt Sinks lie 30 km to the west.

Dixie Meadows hot springs (Figure 1) near the 1954 rupture termination consists of 35 springs and seeps over 4 square miles (10 km^2) with wide variations in temperature and salinity. Springs emerge from alluvium in the hanging wall of the Dixie Valley fault. Temperature and salinity are inversely correlated in these springs suggesting that dissolution of evaporites by cold water and mixing with low salinity hot water accounts for the variation in temperature and salinity [*Bell et al.*, 1980]. Halite-cemented breccias are present in the fault in the vicinity of the hot springs area. Saline, gypsiferous clays occur in the Truckee formation of upper Miocene age in western Nevada [*Morrison*, 1964]. Mixing of cool, salty fluid with higher-temperature, lower-salinity fluids is illustrated by the trend labeled C on Figure 7. A fourth alternative is suggested by continuous displacement of the fault footwall to shallower, cooler depths. This trend is labeled D on Figure 7.

Geothermal fluids at depth in Dixie Valley presently contain CO_2. Fluid in the deep wells contains 312-396 mg/L Na, 37-54 mg/L K, and CO_2 comprises 0.12-0.22 wt % of the fluid (0.09 mol %) at a temperature of 206°-249°C [*Benoit*, 1989]. High bicarbonate in springs emerging from igneous rocks near major faults [*Bohm*, 1984]; vast travertine deposits at Sou hotsprings, 47 km northeast of the 1954 rupture segment; and high bicarbonate (870-936 mg/L at Hyder hot springs, 42 km northeast, may be the result of CO_2 leakage from a deeper geothermal reservoir.

Secondary fluid inclusions in granitic rocks often show final ice melting temperatures in the range below the NaCl-H_2O eutectic [*Konnerup-Madsen*, 1977, 1979]. These types of high-salinity fluids are common in granitic rocks, and their occurrence in healed microfractures in the DixieValley fault rocks together with an intrusive age near the time of inception of Basin and Range extension suggests they may have been important fault fluids.

$CaCl_2$ -NaCl brines have been observed in retrograde Ca-rich amphibolite where retrograde reactions with muscovite, epidote, and chlorite as product minerals are suggested as a mechanism for concentrating Na, K, and Ca in fluids [*Crawford et al.*, 1979]. These Ca-rich compositions are most common in metamorphosed carbonate rich sediments [*Roedder*, 1984, p. 351]. Hydrothermal calcium chloride brines are also known from continental rift systems [*Hardie*, 1990].

FLUID TEMPERATURE AND PRESSURE

Fluid inclusion characteristics and mineral equilibria may be used to place constraints on the fluid pressure and temperature in the Dixie Valley fault footwall. Minimum pressures of entrapment are estimated from CO_2 containing fluid inclusions and from inclusions containing a halite crystal.

The salinity, CO_2 density, and homogenization temperatures of type II fluid inclusions were used together with the CO_2-H_2O-NaCl phase diagram to estimate CO_2 content and minimum pressure of entrapment using the procedures of *Parry* [1986]. Carbon dioxide content ranges from 3 to 17 mol %, and estimated pressures on the two-phase boundary curve for inclusion compositions vary from 280 to 1570 bars. These pressures represent minimum entrapment pressures of a homogenous fluid. Homogenous fluids could have been trapped at higher temperatures and pressures along appropriate isochores for each fluid composition.

Roedder and Bodnar [1980] and *Roedder* [1984] showed that the minimum pressure of entrapment of a homogenous fluid can be estimated from halite-bearing fluid inclusions by first assuming the fluid properties are adequately represented by the NaCl-H_2O system and that NaCl solubility is independent of pressure. The bulk composition of the fluid inclusion fluid and its density were estimated from the melting temperature of NaCl using the regression equation of *Sterner et al.* [1988]. The composition and density of the halite saturated solution on the liquid-vapor curve at the temperature of vapor disappearance were calculated using equations from *Haas* [1976]. At the temperature of liquid-vapor homogenization, the inclusion volume is the volume of saturated solution of known density plus the volume of halite. The mass of halite crystal is obtained from the difference in salinity at the temperature of liquid-vapor homogenization and at the temperature of NaCl melting, and its volume is calculated from halite density. These calculations yield densities of 1.137 and 1.275 g/cm3 for inclusions homogenizing at theNaCl melting temperature of 313° and 356°C, respectively. Extrapolation of the density determinations of *Urusova* [1975] at 350°C to higher pressures indicate a minimum entrapment pressure of about 1500 bars, but extrapolation of the MRK equation of state using the coefficients of *Bowers and Helgeson* [1983] indicates a pressure of 800 bars at 350°C. Extrapolation of *Urusova's* [1975] density measurements to 300°C yields a pressure estimate of 240 bars for the inclusion homogenizing at 313°C.

We next assume that lithostatic pressure represents a reasonable maximum and hydrostatic pressure represents a reasonable minimum for fluid pressure. Second, we infer a thermal gradient so that pressure-temperature gradients maybe shown in Figure 8. The thermal gradient on the Dixie Valley fault is probably greater than the 30°C/km gradient that is characteristic of the Basin and Range Province [*Sass et al.*, 1981]. The northern end of the belt of historic seismicity in the central Nevada seismic belt is an area of conspicuously high heat flow called the Battle Mountain High [*Sass et al.*, 1971] where thermal gradients are 40° to 50°C/km [*Sass et al.* 1981].

Additional indications of elevated geothermal gradients include intense hydrothermal alteration along the range front fault, fumaroles and hot water within 30 m of the surface, As and Hg in soils of the valley near the range front fault [*Juncal and Bell*, 1981], and hot springs widely distributed in the hanging wall of the Dixie Valley fault. The Dixie Valley geothermal area is 47 km northeast of the 1954 rupture segment where gradients of 75°C/km and above have been measured in drill holes [*Bell et al.*, 1980] due to hydrothermal convection. These observations lend support to a thermal gradient in Dixie Valley that exceeds the normal Basin and Range gradient. Lithostatic and hydrostatic pressure gradients are shown on Figure 8 for thermal gradients of 45° and 60°C/km.

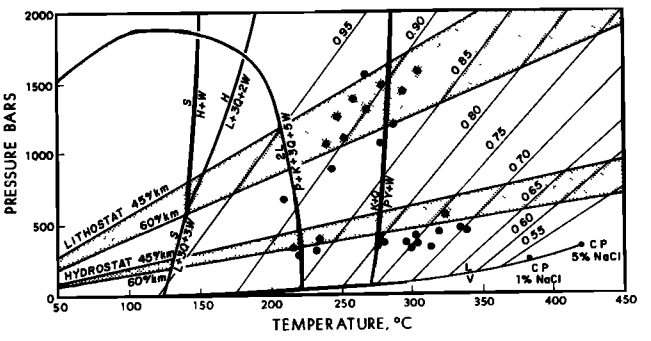

Fig. 8. Minimum pressure and temperature for entrapment of CO_2 fluid inclusions (solid circles), lithostatic and hydrostatic pressure gradients, mineral equilibria, and boiling curves. K, kaolinite; P, pyrophyllite; Q,quartz; W, water; L, laumontite; Pr, prehnite; S, stilbite; H, heulandite. Data for reactions: K+Q=P+W from *Hemley et al.*[1980]; L=Pr+K+3Q+5W from *Bird and Helgeson* [1981]; S=H+W and H=L+3Q+2W from *Cho et al.* [1987]; and S=l+3Q+3W from *Liou* [1971]. Isochores calculated for 1% NaCl solution and various homogenization temperatures from data of *Potter and Brown* [1977]. Boiling curve calculation used data and equations of *Haas* [1976].

A heat source for an elevated gradient is readily available. The earliest phase of extension before 18-15 Ma was synchronous with a generally southward migrating belt of intermediate to silicic volcanism [*Sonder et al.*,1987; *Wernicke et al.*, 1987]. Major Cenozoic igneous activity in the Dixie Valley area began with andesitic lava flows 35 Ma [*Riehle et al.*, 1972]. Voluminous eruptions of quartz latite to rhyolite ash flow tuffs are dated at 32-22 Ma [*Riehle et al.*, 1972; *Speed*, 1976; *Burke and McKee*, 1979]. Basalt flows cap the sequence and have been dated at 13-17 Ma [*Nosker*, 1981]. Small igneous dikes and plutons of latite to diorite occur along the Dixie Valley fault zone. The Dixie Valley fault may be rooted within magmatic intrusion and further intrusion into the crust along the fault might allow for different subsidiary fault displacements and spreading of grabens [*Thompson*, 1966; *Thompson and Burke*, 1974; *Okaya and Thompson*, 1985].

The pressure and temperature of entrapment of type I moderate salinity inclusions must lie on isochores defined by the fluid density. Fluid density is calculated from salinity and homogenization temperature measurements shown in Figure 7. Representative isochores for densities of 0.55 to 0.95 g/cm^3 are shown in Figure 8 corresponding to densities of 1 wt % NaCl solutions that homogenize by vapor disappearance at various temperatures. These fluids would have been trapped along their respective isochores at pressures and temperatures between lithostatic and hydrostatic pressures.

The minimum pressures and temperatures of entrapment of type II, CO_2-bearing inclusions are shown on Figure 8. These fluids, too, would have been trapped on isochores defined by the density of the fluid. The wide range in minimum pressures of entrapment has been interpreted to be the result of pressure transients accompanying dilatant fracturing [*Parry and Bruhn*, 1990]. The highest pressure values are near lithostatic pressure, and the lowest are near hydrostatic pressure.

Additional constraints are placed on P-T conditions by mineral equilibria. Equilibria among kaolinite, pyrophyllite, quartz, and water according to

$$Al_2Si_2O_5(OH)_4 + 2SiO_2 = Al_2Si_4O_{10}(OH)_2 + H_2O \quad (1)$$
(kaolinite) (quartz) (pyrophyllite)

shown on Figure 8 indicate that the presence of kaolinite in these quartz-rich rocks requires temperatures below about 270°C. Pyrophyllite has not been observed despite numerous fluid inclusion homogenization temperatures that exceed 270°C. The reason for this is that fluids contain sufficient K^+ to stabilize muscovite according to

$$3Al_2Si_4O_{10}(OH)_2 + 2K^+ = 2KAl_3Si_3O_{10}(OH)_2 + 2H_+. \quad (2)$$
(pyrophyllite) (muscovite)

The low-temperature stability of epidote in the presence of quartz and an aqueous solution at pressures between 500 and 3800 bars is represented by reaction (3) [*Bird and Helgeson*, 1981]. Prehnite is stable relative to laumontite above about 220°C (reaction (4)) and stilbite is stable relative to laumontite below about 130°-140°C at pressures below 600 bars (reaction(5)):

$$2Ca_2Al(AlSi_3O_{10}(OH)_2 + Al_2Si_2O_5(OH)_4$$
(prehnite) (kaolinite)

$$=2Ca_2Al_3Si_3O_{12}(OH) + 2SiO_2 + 3H_2O \quad (3)$$
(epidote) (quartz)

$$2CaAl_2Si_4O_{12}.4H_2O$$
(laumontite)

$$=Ca_2Al(AlSi_3O_{10}(OH)_2 + Al_2Si_2O_5(OH)_4 + 3SiO_2 + 5H_2O \quad (4)$$
(prehnite) (kaolinite) (quartz)

$$CaAl_2Si_7O_{18}.7H_2O = CaAl_2Si_4O_{12}.4H_2O + 3SiO_2 + 3H_2O \quad (5)$$
(stilbite) (laumontite) (quartz)

Examination of equilibria (1), (4), and (5) on Figure 8 shows that mineral assemblages along with fluid inclusion properties record a systematic decrease in both temperature and pressure with displacement of the footwall during faulting. Fluid temperature at depth on the fault exceeded 350°C and pressure exceeded 1500 bars. K-feldspar, biotite, epidote, chlorite, and muscovite were the earliest formed stable mineral phases. As temperature and pressure decreased, kaolinite was stabilized relative to muscovite and pyrophyllite below about 270°C, prehnite was stabilized relative to epidote and then laumontite was stabilized relative to prehnite at about 220°C. At 140°C, stilbite is stable relative to laumontite and the fluid pressure must be lower than 600 bars, otherwise heulandite would occur. As pressure and temperature decreased, CO_2 separated so that zeolites were stabilized relative to calcite and clay.

REGIONAL IMPLICATIONS

The Stillwater Range lies in part of a regional WNW trending belt of mostly silicic volcanism that extended across southern Nevada from late Eocene through early Miocene time. This belt was characterized by widespread hydrothermal alteration and NW to WNW structural trends that included numerous dikes, caldera complexes, and high-angle fault and joint systems [*Boden*, 1986]. In some locales, NE rending faults formed as subsidiary features [*Rielhe et al.*, 1972; *Boden*, 1986; *Hudson and Geissman*, 1987]. *Hudson and Geissman* [1987] noted that counterclockwise rotation of rocks in the central Stillwater Range and Clan Alpine Mountains occurred as the result of movement on a complex array of strike-slip, oblique-slip, and dip-slip faults and suggested that rotation was accomplished by movement on NW-striking, right-lateral faults. *Li et al.* [1990] see paleomagnetic evidence for counterclockwise block rotations elsewhere in northern Nevada.

Regional extension in the great Basin dates from about 30 Ma and occurred in two episodes. The early episode of extension in northern Nevada was oriented S68°W-N68°E. At about 10 Ma the extension direction changed by clockwise rotation to the present-day extension direction of N65°W-S65°E [*Zoback et al.*, 1981; *Zoback and Thompson*, 1978; *Eaton*, 1982]. The early phase of extension dated at 23-15 Ma based on angular unconformity and rotated high angle faults [*John et al.*, 1989] was accommodated by rotation of crustal blocks, strike slip motion on northwest trending faults, and normal faults that predate widespread basaltic volcanism dated at 13 to 17 Ma [*Hudson and Geissman*, 1987]. Remnants of this NW striking right-lateral fault set were preserved in the interior of the Stillwater Range near White Rock Canyon and Coyote Canyon and may be represented by the western fault branch in the "bend", within the present-day Dixie Valley fault zone (Figure 9). Hydrothermal activity and tectonic displacement on at least part of the Dixie Valley fault began during this early stage of extension. K/Ar ages of hydrothermal sericite on the fault are 21.8 to 25 Ma (Table 1) and mineral-filled veins and fluid inclusion train orientations are consistent with the earlier extension direction. The orientation and age of hydrothermal minerals in the older, NW to WNW trending vein arrays indicate that these features probably reflect Oligocene to early Miocene deformation and hydrothermal activity, which occurred prior to the onset of NNE trending Basin and Range normal faulting [*Stewart et al.*, 1977].

The later episode of extension beginning at 10-13 Ma [*Eddington et al.*, 1987; *Zoback et al.*, 1981] is indicated by 10 Ma old basalt on the west flank of Job Peak that is tilted 10° west [*Wallace and Whitney*, 1984]. Basalt and andesite cap the Stillwater range at an elevation of 2200 m and also produce seismic reflections in Dixie Valley at an elevation 1280 m below sea level for a total of post-13-17 Ma displacement on the fault of 3.5 km [*Wallace and Whitney*, 1984] to 2.2 km farther north [*Okaya and Thompson*,1985].

Moderate salinity fluid inclusions were trapped at the pressure and temperature defined by the isochore for the fluid density illustrated on Figure 8. Fluid inclusions containing CO_2 were trapped at minimum pressures as high as 1570 bars at a temperature of 305°C (Table 3) shown in Figure 8 and corresponding to a lithostatic pressure at a depth of over 6 km. Aqueous fluid inclusions that homogenize at 380°-400°C then if trapped no deeper than 6 km must have been trapped at a thermal gradient of nearly 70°C/km.

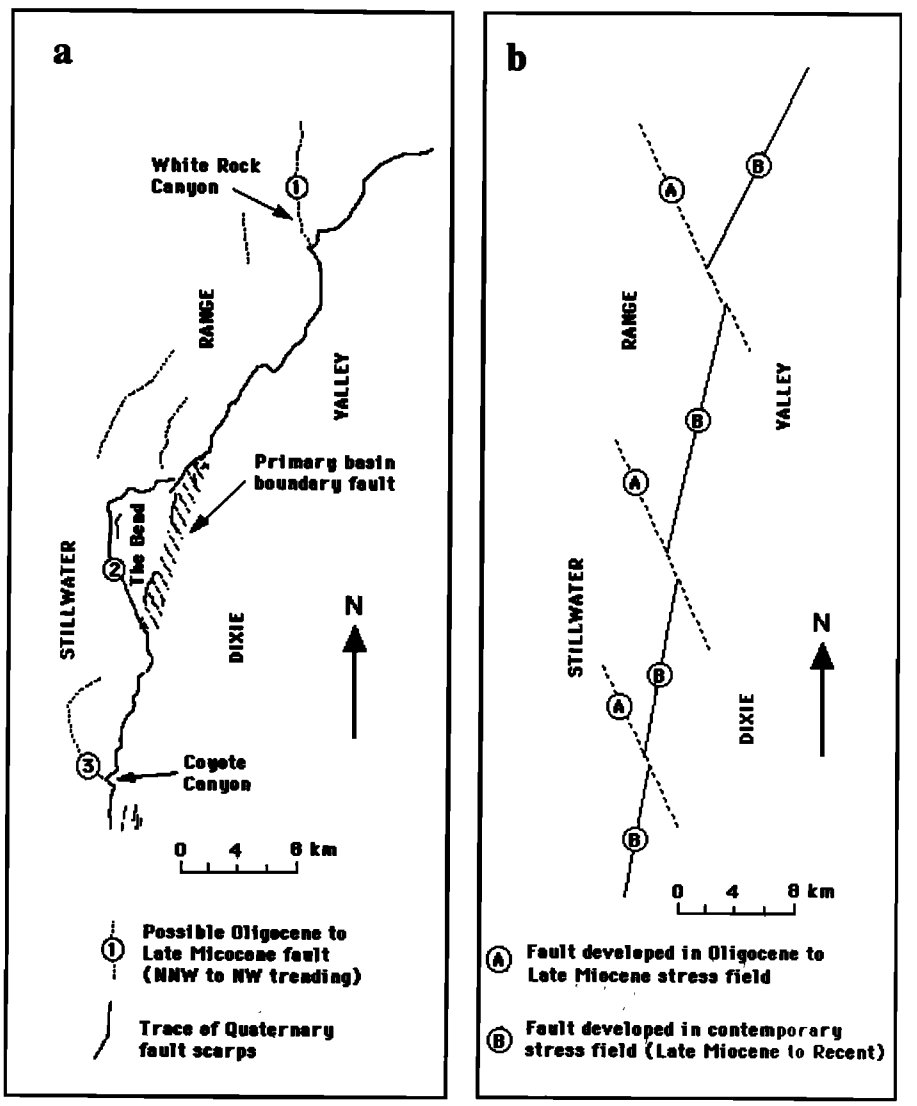

Fig. 9. (a) Map view of the rupture trace of the Dixie Valley fault. Localities referred to in the text are 1, White Rock Canyon; 2, The Bend; and 3, Coyote Canyon. (b) Map view of proposed development of the Dixie Valley fault from superposition of faults developed in contemporary stress field on Oligocene to late Miocene faults.

Supporting geological evidence for prebasalt displacement is evident on the 1:125,000 scale map of *Page* [1965] and the 1:250,000 scale map of *Willden and Speed* [1974]. Volcanic rock units on these maps include older Tertiary latite welded tuffs 0.6-1.8 km thick that are overlain by rhyolite to rhyodacite welded tuffs 0.6-3.0 km thick and rhyolite to rhyodacite. Basalt on the west flank of Job Peak directly overlies the older latite welded tuffs. Rhyolite to rhyodacite and up to 3.0 km of rhyodacite welded tuffs are missing. The older latite welded tuffs are exposed along a series of north to NW striking faults. Farther north, the basalt is in contact with Jurassic volcanics; rhyolite to rhyodacite, up to 3.0 km of rhyodacite welded tuffs, and 0.6 to 1.8 km of latite welded tuffs are missing. The older rock units are exposed on north to NW trending faults. The footwall of the Dixie Valley fault in the area C to D of Figure 1 also trends north to NW. Here Tertiary plutons have been unroofed, a Cretaceous pluton at D has been unroofed and the entire sequence of Tertiary volcanic rocks is missing exposing Mesozoic sedimentary rocks.

Evidence suggest that the present-day Dixie Valley fault zone began to form during Oligocene to early Miocene time and may have undergone two phases of extension. First, the fact that sericite-clay and older alteration mineral assemblages occur in a narrow band along the present-day fault trace suggests that a zone of intense fracturing and hydrothermal alteration with a geometry roughly similar to that of the Quaternary fault zone formed during Oligocene to early Miocene time. Second, paleofluid entrapment pressures estimated from measurements of high-temperature fluid inclusions indicate a minimum footwall uplift of 6 km. This is 3-4 km more vertical displacement than the post-13-17 ma displacement estimate of 3.5-2.2 km [*Wallace and Whitney*, 1984; *Okaya and Thompson*, 1985], suggesting that the early phase of vertical displacement was similar in magnitude to that of the later phase. Notably, the post-13-17 Ma displacement is estimated from offset of basalts that were extruded over a fairly flat surface. A period of tectonic quiescence must have occurred between the early and later phases of extension across the DixieValley fault zone. Third, we note that the Dixie Valley fault trace is highly sinuous, with two strong maxima in fault strike, one toward the WNW to NNW and the other NNE to NE (Figure 9). Perhaps this pattern is partly inherited from the earlier, Oligocene to early Miocene phase of extension,when deformation was concentrated on WNW striking strike-slip faults and subsidiary normal and normal-oblique-slip faults, many of which trended NNE to NE, forming a rectangular fault pattern when observed in map view [*Riehle* et al., 1972; *Hudson and Geissman*, 1987; *Boden*, 1986]. Presumably, rotation of extension from N68°E to S65°E about 10 Ma enhanced movement on NNE to NE trending normal faults, relative to older sets of WNW to NNW trending faults. Nevertheless, the distribution of hydrothermal alteration minerals, and the internal structure of the Dixie Valley fault zone indicate that part of the overall structural geometry is inherited from Oligocene and early Miocene deformation and hydrothermal circulation.

COMPARISONS WITH CONTEMPORARY FAULTS

Two well-studied contemporary fault systems in the Great Basin provide valuable comparisons. The Wasatch fault in the eastern Great Basin [*Parry and Bruhn*, 1986; *Parry et al.*,1988] and the Nevada Comstock fault in western Nevada [*Vikre*, 1989] are normal faults with displacement histories beginning in the Miocene.

Exhumation of the footwall at the southern end of the Salt Lake segment of the Wasatch fault has exposed hydrothermally altered granitic rocks. Vein filling and pervasive alteration mineralogy includes, from earliest to latest, biotite-K-feldspar, chlorite-epidote-sericite, and laumontite-prehnite-clay. Secondary fluid inclusions present in healed fractures in quartz associated with syntectonic chlorite-epidote-sericite alteration contain 3 to 32 mol % CO_2 with 4.5 to 17.3 wt % NaCl solution. The mode of homogenization temperatures is 285°C. Estimated minimum entrapment pressures vary from 600 to 2950 bars. The mode of homogenization temperatures of secondary inclusions associated with the later laumontite-prehnite assemblage is 100°C, salinity ranges from 2.0 to 16.0 NaCl equivalent wt %, and no CO_2 was detected.

Fluid pressure and temperature within this segment of the Wasatch fault evolved along a path from lithostatic to hydrostatic with continued displacement of the footwall relative to the hanging wall. Age constraints are provided by a 17.6±0.6 Ma K-Ar age of hydrothermal sericite from a sample with mean Th of 309°C, and 7.3 to 9.6 Ma fission track ages of apatite (closure temperature 120°±15°C). Temperature and pressure estimates suggest post-17.6 Ma fault displacement is 11 km at a thermal gradient of 30°C/km [*Parry and Bruhn*, 1987].

The major tectonic consequence of the pore fluid and chemical reactions observed on the Wasatch fault is reduction of effective stress by pore fluid pressure. Elevated pressures are enhanced by chemical reactions that seal the tectonically induced cracks in the rock. The mechanical behavior of the rock is also modified by formation of chlorite and sericite with epidote in the fault rock at deeper levels, and vein fillings of zeolite, calcite, and clay minerals at shallower levels.

A contemporary fault system that has been examined in detail due to bonanza economic mineralization, the Comstock fault at Virginia City, Nevada, shows many similarities to the Dixie Valley fault. The Comstock fault is a major mineralized crustal structure 135 km southwest of Dixie Valley. This fault displaces Miocene volcanic rocks 762-1219 m [*Vikre et al.*, 1988] and is mineralized over 4.6 km of strike length and to 1000 m below the present surface. Post-Miocene displacement is less than 183 m, and the fault is not presently active. Fault-related alteration and fluid characteristics date from the earlier episode of Basin and Range extension without superimposition of younger hydrothermal events. Alteration which is associated with precious metal veins and the Comstock fault includes strong silicification adjacent to the Comstock fault with accompanying sericite, chlorite, and pyrite. Near lode margins quartz, sericite, chlorite,montmorillonite, and pyrite overlie quartz + sulfide lodes. K-feldspar, albite, sericite, chlorite, and calcite locally occur with sulfides.

Chlorite, calcite, epidote, albite, quartz, and pyrite comprise a propylitic assemblage with no close association to the Comstock fault. A younger albite, natrolite, stilbite assemblage, and an assemblage of quartz, alunite, pyrophyllite, and clay are also not fault related.

Fluids circulated at least 2000 m below the Miocene paleosurface at temperatures from about 250°-300°C, with salinities of 1-6 % NaCl and up to 2.1 wt % CO_2. Fluids with recognizable CO_2 contain <3.2% NaCl, fluids with no CO_2 contain 0.4-6.1 % NaCl, and fluid inclusions with daughter NaCl and KCl contain 23% NaCl and 47% KCl. Boiling and mixing were invoked by *Vikre* [1989] to account for variable solution compositions, but the CO_2-bearing inclusions were determined to be later than those with no CO_2.

The Wasatch, Dixie Valley, and Comstock faults share several common characteristics. Fault fluids contain disolved salts and CO_2, homogenization temperature modes are 250°-300°C. Fluid pressures on the Wasatch and Dixie Valley faults varied between lithostatic and hydrostatic pressures. Alteration minerals in the footwall include the common assemblages chlorite, epidote, sericite, prehnite, laumontite, zeolite, silicification, and clay.

CONCLUSIONS

Detailed mapping, petrographic, and fluid inclusion work on the Dixie Valley fault and comparison with the Wasatch fault and Comstock fault suggests a model for Basin and Range seismogenic faults from which the relationship of fault behavior to fluid characteristics can be derived.

Hydrothermally altered footwall rocks have been exhumed by fault displacement and erosion on the Dixie Valley Fault, Nevada. Much of the footwall of the 1954 rupture segment consists of Tertiary age granitic rocks that provide alumino-silicate parent minerals for the alteration and constrain the maximum age of the alteration to be less than 28 Ma. Overlapping episodes of hydrothermal mineral formation were produced as displacement of the fault progressed. These mineral assemblages are from earliest to latest: hydrothermal biotite+K-feldspar, chlorite+epidote, sericite+kaolinite+smectite, prehnite+laumontite+stilbite+clay, and chalcedony, opal, smectite, alunite,and kaolinite. Microthermometric measurement of fluid inclusion characteristics indicate a diverse fluid chemistry, temperature, and pressure of entrapment. Hydrothermal alteration minerals and characteristics of secondary fluid inclusions trapped in healed microfractures in igneous quartz place constraints on fluid pressure and temperature during faulting.

Fluid inclusions in hydrothermally altered footwall rocks of the Dixie Valley fault, Nevada indicate that pore fluid pressure fluctuated from 1570 to 350 bars in the temperature range 350°-200°C. Scatter in the pressure estimates at constant temperature is interpreted as paleo-fluid pressure transients at depths of up to 3-5 km on the Dixie Valley fault. The pressure transients are greatest in the temperature range 270°-310°C.

Interaction of the pore fluid with host rock quartz monzonite on the Dixie Valley fault has resulted in a series of temperature dependent chemical reactions producing minerals that seal fractures and alter the mechanical properties of the rock. Ductile deformation combined with hydrothermal crack sealing must effectively prevent fluid communication with near surface fluids. As deformation becomes more brittle, rock fractures are less effectively sealed, the decrease in confining pressure allows fractures to be more open, and fluid pressures drop to hydrostatic conditions. Upward displacement of footwall rocks and decreasing fluid pressure permit open system conditions, effervescence of CO_2, and precipitation of calcite, zeolite, and other minerals in rock fractures.

Fault domains at a depth of up to 5 km on the Dixie Valley fault containing a CO_2-rich fluid may play a key role in nucleation and propagation of earthquake ruptures. Ruptures may be initiated by high pore pressures caused by porosity reduction. New pore volume produced by dilatancy coupled with low rock permeability would then result in decompression of the fluid and may stabilize the rupture by dilatant hardening. The dilatant hardening effect is proportional to the coefficient of friction and the pore fluid bulk modulus, $(\rho\ dP/d\rho)_T$, where ρ is density, P is pressure, and T is temperature [*Rudnicki and Chen*, 1988]. Separation of CO_2-H_2O-NaCl fluids into two phases drastically reduces the fluid bulk modulus that diminishes the dilatant hardening effect and permits ruptures to propagate [*Parry and Bruhn*, 1990].

Acknowledgments. Financial support was provided by NSF grant EAR-8618250 to R.L.B. and W.T.P. The manuscript was carefully reviewed by Paula N. Wilson, John R. Bowman, and Ricardo Presnell. We are grateful to JGR reviewers E. Roedder and G. A. Thompson for their many helpful comments.

REFERENCES

Anderson, R. E., M. L. Zoback, and G. A. Thompson, Implications of selected subsurface data on the structural form and evolution of some basins in the northern Basin and Range province, Nevada and Utah, *Geol. Soc. Am. Bull.*, *94*, 1055-1072, 1983.

Bateman, R. L., and J. W. Hess, Hydrologic inventory and evaluation of Nevada playas, *Proj. Rep. 49*, 137 pp, Water Resour. Cent., Desert Res. Inst., Univ. of Nev., Las Vegas, 1978.

Bell, E. J., et al., Geothermal reservoir assessment case study, northern Basin and Range province, northern Dixie Valley, Nevada, report, 223 pp., Mackay Miner. Res. Inst., Univ. of Nev., Reno, 1980.

Bell, J. W. and T. Katzer, Surficial geology, hydrology, and late Quaternary tectonics of the IXL Canyon area, Nevada, *Bull. Nev. Bur. Mines Geol. 102*, 51 pp., 1987.

Bell, J. W., and T. Katzer, Timing of late Quaternary faulting in the 1954 Dixie Valley earthquake area, central Nevada, *Geology*, *18*, 622-625, 1990.

Benoit, W. R., Carbonate scaling characteristics in Dixie Valley, Nevada geothermal well bores, *Geothermics*, *18*, 41-48, 1989.

Bird, D. K., and H. C. Helgeson, Chemical interaction of aqueous solutions with epidote-feldspar mineral assemblages in geologic systems, II, Equilibrium constraints in metamorphic/geothermal processes, *Am. J. Sci.*, *281*, 576-614, 1981.

Boden, D. R., Eruptive history and structural development of the Toquima caldera complex, central Nevada, *Geol. Soc. Am. Bull.*, *97*, 61-74, 1986.

Bodnar R. J., T. J. Reynolds, and C. A. Kuehn, Fluid-inclusion systematics in epithermal systems, in *Geology and Geochemistry of Epithermal Systems, Rev. Econ. Geol.*, vol. 2, edited by. B.R. Berger and P. M. Bethke, pp. 73-97,.Society of Economic Geologists, El Paso, Tex.,1985.

Bohm, B., Possible relations between anomalous spring water chemistry in the Stillwater Range, and the Dixie Valley geothermal system, northern Nevada, *Trans. Geotherm. Resour. Counc.*, *8*, 369-371, 1984.

Bowers T. S. and H. C. Helgeson, Calculation of the thermodynamic and geochemical consequences of nonideal mixing in the system H_2O-CO_2-NaCl on phase relations in geologic systems: Equation of state for H_2O-CO_2-NaCl fluids at high pressures and temperatures, *Geochim. Cosmochim. Acta*, *47*, 1247-1275, 1983.

Bozzo A. T., H-S Chen, J. R. Kass, and A. J. Barduhn, The properties of the hydrates of chlorine and carbon dioxide, *Desalination*, *16*, 303-320, 1975.

Burke, D. B., and E. H. McKee, Mid-Cenozoic volcano-tectonic troughs in central Nevada, *Geol. Soc. Am. Bull.*, *90*, 181-184, 1979.

Cho, M., S. Maruyama, and J. G. Liou, An experimental investigation of heulandite-laumontite equilibrium at 1000 to 2000 bar P fluid, *Contrib. Mineral. Petrol.*, *97*, 43-50, 1987.

Collins, P. L. F., Gas hydrates in CO_2-bearing fluid inclusions and the use of freezing for estimation of salinity, *Econ. Geol.*, *74*, 1435-1444, 1979.

Crawford, M. L., J. Filer, and C. Wood, Saline fluid inclusions associated with retrograde metamorphism, *Bull. Mineral.*, *102*, 562-568, 1979.

Eaton, G. P., The Basin and Range province: Origin and tectonic significance, *Annu. Rev. Earth Planet. Sci.*, *10*, 409-440, 1982.

Eddington, P. K., R. B. Smith, and C. Renggli, Kinematics of Basin and Range intraplate extension, in Continental Extensional Tectonics, edited by M. P. Coward, J. F. Dewey, and P. L. Hancock, *Geol. Soc. Spec. Pub. London*, *28*, 371-392, 1987.

Haas, J. L., Jr., Physical properties of the coexisting phases and thermochemical properties of the H_2O component in boiling NaCl solutions, *U. S. Geol. Surv. Bull.*, *1421-A*, 73 pp., 1976.

Hardie, L. A., The roles of rifting and hydrothermal $CaCl_2$ brines in the origin of potash evaporites: An hypothesis, *Am. J. Sci.*, *290*, 43-106, 1990.

Hemley, J. H., J. W. Montoya, J. W. Marinenko, and R. W. Luce, Equilibria in the system Al_2O_3-SiO_2-H_2O and some general implications for alteration/mineralization processes, *Econ. Geol.*, *75*, 210-228, 1980.

Hubbert, M. K. and W. W. Rubey, Role of fluid pressure in the mechanics of overthrust faulting, *Geol. Soc. of Am. Bull.*, *70*, 115-205, 1959.

Hudson, M. R., and J. W. Geissman, Paleomagnetic and structural evidence for middle Tertiary counterclockwise block rotation in the Dixie Valley region, west-central Nevada, *Geology*, *15*, 638-642, 1987.

Ismail, I. A. H., and S. A. F. Murrell, Dilatancy and the strength of rocks containing pore water under undrained conditions., *Geophys, J. R. Astron. Soc.*, *44*, 107-136, 1976.

Janecke, S. U., and J. P. Evans, Feldspar-influenced rock rheologies, *Geology*, *16*, 1064-1067, 1988.

John, D. A., R. E. Thomason, and E. H. McKee, Geology and K-Ar geochronology of the Paradise Peak mine and the relationship of pre-Basin and Range extension to early Miocene precious metal mineralization in west central Nevada, *Econ. Geol.*, *84*, 631-649, 1989.

Juncal, R. W., and E. J. Bell, Solid-sample geochemistry study of western Dixie Valley, Churchill County, Nevada, part II, Soil geochemistry, *Trans. Geotherm. Resour. Counc.*, *5*, 51-54, 1981.

Kamb, W. B., Petrofabric observations from Blue Glacier, Washington, in relation to theory and experiment, *J. Geophys. Res.*, *64*, 1891-1909, 1959.

Kirby, S. H. and A. K. Kronenberg, Rheology of the lithosphere: Selected topics, *Rev. Geophys.*, *25*, 1219-1244, 1987.

Konnerup-Madsen, J., Composition and microthermometry of fluid inclusions in the Kleivan granite, south Norway, *Am. J. Sci.*, *277*, 673-696, 1977.

Konnerup-Madsen, J., Fluid inclusions in quartz from deep-seated granitic intrusions, south Norway, *Lithos*, *12*, 13-23, 1979.

Li, Y., J. W. Geissman, A. Nur, R. Hagai, and Q. Huang, Paleomagnetic evidence for counter clockwise block rotation in the north Nevada rift region, *Geology*, *18*, 79-82, 1990.

Liou, J. G., Stilbite-laumontite equilibrium, *Contrib. Mineral. Petrol.*, *31*, 171-177, 1971.

Meister, L. J., Seismic refraction study of Dixie Valley, Nevada, Ph. D. thesis, 72 pp., Stanford Univ., Stanford, Calif., 1967.

Morrison, R. B., Lake Lahontan: Geology of the southern Carson Desert, Nevada, *U.S. Geol. Surv. Prof. Pap.*, *401*, 156 pp., 1964.

Nosker, S. A., Stratigraphy and structure of the Sou Hills, Pershing County, Nevada, M. S. Thesis, 60 pp., Univ. of Nev., Reno, 1981.

Oakes, C. S., R. J. Bodnar, and J. M. Simonson, The system NaCl-$CaCl_2$-H_2O, I, The ice liquidus at 1 atm total pressure, *Geochim. Cosmochim. Acta*, *54*, 603-610, 1990.

Okaya, D. A., and G. A. Thompson, Geometry of Cenozoic extensional faulting: Dixie Valley, Nevada, *Tectonics*, *4*, 107-125, 1985.

Page, B. M., Preliminary geologic map of a part of the Stillwater Range, Churchill County, Nevada, *Map 28*, Nev. Bur. of Mines and Geol., Reno, 1965.

Parry, W. T., Estimation of XCO_2, P, and fluid inclusion volume from fluid inclusion temperature measurements in the system NaCl-CO_2-H_2O, *Econ. Geol.*, *81*, 1009-1013, 1986.

Parry W. T., and R. L Bruhn, Pore fluid and seismogenic characteristics of fault rock at depth on the Wasatch fault, Utah, *J. Geophys. Res.*, *91*, 730-744, 1986.

Parry, W. T., and R. L. Bruhn, Fluid inclusion evidence for minimum 11 km vertical offset on the Wasatch fault, Utah, *Geology*, *15*, 67-70, 1987.

Parry, W. T., and R. L. Bruhn, Fluid pressure transients on seismogenic normal faults, *Tectonophysics*, *179*, 335-344, 1990.

Parry, W. T., P. N. Wilson, and R. L. Bruhn, Pore-fluid chemistry and chemical reactions on the Wasatch normal fault, Utah, *Geochim. et Cosmochim. Acta*, *52*, 2053-2063, 1988.

Potter, R. W., II, and D. L. Brown, The volumetric properties of aqueous sodium chloride solutions from O°C to 500°C at pressures up to 2000 bars based on regression of available data in the literature, *U.S. Geol. Surv. Bull.*, *1421-C*, 36 pp., 1977.

Potter R. W. II, M. A. Clynne, and D. L. Brown, Freezing point depression of aqueous sodium chloride solutions, *Econ. Geol.*, *73*, 284-285, 1978.

Riehle, J. R., E. H. McKee, and R. C. Speed, Tertiary volcanic center, west-central Nevada, *Geol. Soc. of Am. Bull.*, *83*, 1383-1396, 1972.

Roedder E., Fluid inclusions, *Rev. Mineral.*, *12*, 644 pp, 1984.

Roedder, E., and R. J. Bodnar, Geologic pressure determinations from fluid inclusion studies, *Annu. Rev. Earth Planet. Sci.*, *8*, 263-301, 1980.

Roeloffs, E., and J. W. Rudnicki, Coupled-deformation diffusion effects on water level changes due to propagating creep events, *Pure Appl. Geophys.*, *122*, 560-582, 1985.

Rudnicki, J. W., and C. J. Chen, Stabilization of rapid frictional slip on a weakening fault by dilatant hardening, *J. Geophys. Res.*, *93*, 4745-4757, 1988.

Sass, J. H., A. H. Lachenbruch, R. H Monroe, G. W. Greene, and T. J. Moses, Jr, Heat flow in the western United States, *J. Geophys. Res.*, *76*, 6376-6413, 1971.

Sass, J. H., D. D. Blackwell, D. S. Chapman, J. K. Costain, E. R. Decker, L. A. Lawver, and C. A. Swanberg, Heat flow from the crust of the Unites States, in *Physical Properties of Rocks and Minerals, McGraw-Hill/CINDAS Data Ser. on Mater. Prop.* Vol. II-2, edited by Y. S. Touloukian, W. R. Judd, and R. F. Roy, pp. 5681-5698, McGraw-Hill, New York, 1981.

Sibson, R. H., Controls on low-stress hydro-fracture dilatancy in thrust, wrench and normal fault terrains, *Nature*, *289*, 665-667, 1981.

Sibson, R. H., Fluid flow accompanying faulting: Field evidence and models, in *Earthquake Prediction: An International Review, Maurice Ewing Ser.* vol. 4, edited by D. W. Simpson and P. G. Richards, pp. 593-603, AGU, Washington, D. C., 1981.

Sibson, R. H., F. Robert, and K. H. Poulson, High-angle reverse faults, fluid-pressure cycling, and mesothermal gold-quartz deposits, *Geology*, *16*, 551-555, 1988.

Sonder, L. J., P. C. England, B. P. Wernicke, and R. L. Christiansen, A physical model for Cenozoic extension of western North America, in Continental Extensional Tectonics, edited by M. P. Coward, J. F. Dewey, and P. L. Hancock, *Geol. Soc. London Spec. Publ. 28*, 187-201, 1987.

Speed, R. C., Geologic map of the Humboldt Lopolith, scale 1:81050, *Map Chart Ser.MC-14*, Geol. Soc. of Am. Boulder, Colo., 1976.

Speed, R. C., and R. L. Armstrong, Potassium-argon ages of some minerals from igneous rocks of western Nevada, *IsochronWest*, *71*(1), 1-8, 1971.

Sterner S. M., and R. J. Bodnar, Synthetic fluid inclusions in natural quartz, I, Compositional types synthesized and applications to experimental geochemistry, *Geochim. Cosmochim. Acta*, *48*, 2659-2668, 1984.

Sterner, S. M., D. L. Hall, and R. J. Bodnar, Synthetic fluid inclusions, V, Solubility relations in the system NaCl-KCl-H_2O under vapor saturated conditions, *Geochim. Cosmochim. Acta*, *52*, 989-1005, 1988.

Stewart, J. H., Geology of Nevada, *Spec. Publ. 4*, 136 pp., Nev. Bur. of Mines and Geol., Reno, 1980.

Stewart, J. H., W. J. Moore, and I. Zeitz, East-west patterns of Cenozoic igneous rocks, aeromagnetic anomalies, and mineral deposits, Nevada and Utah, *Geol. Soc. Am. Bull.*, *88*, 67-77, 1977.

Thompson, G. A., The rift system of the western United States, in The World Rift System edited by T. N. Irvine, *Tech Surv. Pap.* 66-14, pp. 280-290, Geol. Surv. Can. Dep. of Mines, Ottawa, 1966.

Thompson, G. A., Perspective from the Fairview Peak-Dixie Valley earthquakes of 1954, in Proceedings of Workshop XXVIII on the Borah Peak Earthquake, edited by R. S. Stein and R. C. Bucknam, *U.S.Geol. Surv. Open File Rep.*, *85-290*, 27-42, 1985.

Thompson, G. A., and D. B. Burke, Rate and direction of spreading in Dixie Valley, Basin and Range province, Nevada, *Geol. Soc. Am. Bull.*, *84*, 627-632, 1973.

Thompson, G. A., and D. B. Burke, Regional geophysics of the Basin and Range province, *Annu. Rev. Earth Planet. Sci.*, 2, 213-238, 1974.

Urusova, M. A., Volume properties of aqueous solutions of sodium chloride at elevated temperatures and pressures, *Russ. J. of Inorg. Chem.* Engl. Trans., *20*, 1717-1721, 1975.

Vikre, P. G., Fluid-mineral relations in the Comstock lode, *Econ. Geol.*, *84*, 1574-1613, 1989.

Vikre, P. G., E. H. McKee, and M. L. Silberman, Chronology of Miocene hydrothermal and igneous events in the western Virginia Range, Washoe, Storey, and Lyon counties, Nevada, *Econ. Geol.*, *83*, 864-874, 1988.

Wallace, R. E., Patterns and timing of late Quaternary faulting in the Great Basin province and relation to some regional tectonic features, *J. Geophys. Res.*, *89*, 5763-5769, 1984.

Wallace, R. E., and R. A. Whitney, Late Quaternary history of the Stillwater seismic gap, Nevada, *Bull. Seismol. Soc. Am.*, *74*, 301-314, 1984.

Wernicke, B. P., R. L. Christiansen, P. C. England, and L. J. Sonder, Tectonomagmatic evolution of Cenozoic extension in the North American Cordillera in Continental Extensional Tectonics, edited by M. P. Coward, J. F. Dewey, and P. L. Hancock, *Geol. Soc. Spec. Publ. London*, *28*, 203-221, 1987.

Willden, R., and R. C. Speed, Geology and mineral resources of Churchill County, Nevada, *Nev. Bur. Mines Geol. Bull 83*, 95 pp., 1974.

Zoback, M. L., and G. A. Thompson, Basin and Range rifting in northern Nevada: Clues from a mid-Miocene rift and its subsequent offsets, *Geology*, *6*, 111-116, 1978.

Zoback, M. L., R. E. Anderson, and G. A. Thompson, Cainozoic evolution of the state of stress and style of tectonism of the Basin and Range province of the western United States, *Philos. Trans. R. Soc. London, Series A*, *300*, 407-434 ,1981.

W. T. Parry, D. Hedderly-Smith, and R. L Bruhn, Department of Geology and Geophysics, Unitersity of Utah, Salt Lake City, UT 84112.

(Received February 1, 1991;
revised June 26, 1991;
accepted July 22, 1991.)